inorganics

MDPI

Article

Chalcogen Bonds, Halogen Bonds and Halogen···Halogen Contacts in Di- and Tri-iododiorganyltellurium(IV) Derivatives

Sergi Burguera, Rosa M. Gomila, Antonio Bauzá and Antonio Frontera *

Departament de Química, Universitat de les Illes Balears, Crta de Valldemossa km 7.5, 07122 Palma de Mallorca, Spain; sergi.burguera@uib.es (S.B.); rosa.gomila@uib.es (R.M.G.); antonio.bauza@uib.es (A.B.)

* Correspondence: toni.frontera@uib.es

Abstract: In this manuscript, we have examined the CSD (Cambridge Structural Database) to investigate the relative ability of Te and I (in practice, the heaviest chalcogen and halogen atoms) in di- and tri-iododiorganyltellurium(IV) derivatives to establish σ-hole interactions. The geometry around the Te(IV) in this type of compound is trigonal bipyramidal where the stereoactive lone pair at Te(IV) occupies one of the equatorial positions. In the solid state, Te(IV) tends to form pseudo-octahedral coordination by establishing strong noncovalent interactions opposite to the two covalent bonds of the equatorial plane. Such contacts can also be classified as chalcogen bonds following the recommendation of the International Union of Pure and Applied Chemistry (IUPAC). Such contacts have been analyzed energetically in this work using density functional theory (DFT) calculations, rationalized using molecular electrostatic potential (MEP) surface analysis and characterized using a combination of the quantum theory of atoms in molecules (QTAIM) and noncovalent interaction plot (NCIplot) computational tools. Finally, the observation of halogen bonds and type I halogen···halogen contacts is also emphasized and compared to the chalcogen bonds. Energy decomposition analysis has also been performed to compare the physical nature of chalcogen, halogen and type I interactions.

Keywords: chalcogen bonds; halogen bonds; halogen···halogen contacts; σ-hole interactions; DFT calculations; CSD survey

Citation: Burguera, S.; Gomila, R.M.; Bauzá, A.; Frontera, A. Chalcogen Bonds, Halogen Bonds and Halogen···Halogen Contacts in Di- and Tri-iododiorganyltellurium(IV) Derivatives. *Inorganics* **2023**, *11*, 209. https://doi.org/10.3390/inorganics11050209

Academic Editor: Moris S. Eisen

Received: 1 May 2023
Revised: 10 May 2023
Accepted: 11 May 2023
Published: 12 May 2023

1. Introduction

Sigma–hole (σ-hole) interactions are noncovalent interactions that involve the formation of a weak bond between an electron-deficient atom (typically a group 14–17 element) and a nucleophile, which is usually an electron-rich atom or a molecule [1–9]. The electron-deficient atom (X) is usually attached to an electron-withdrawing group (EWG) and has a region of positive electrostatic potential (σ-hole) opposite to the EWG–X covalent bond that can attract the nucleophile [10–25]. This type of interaction is often named by using the name of the group the electrophilic atom belongs to (e.g., halogen bond for X = chlorine, bromine or iodine) [21]. These interactions have been observed in a variety of chemical and biological systems, and they play a significant role in molecular recognition, crystal engineering and drug design [26–32].

Chalcogen bonding (ChB) is a sub-class of σ-hole interactions that has recently been defined by the IUPAC [2], and it is similar to that of a halogen bond [1]. Similarly to other σ-hole interactions, chalcogen bonding involves the formation of a noncovalent bond between the nucleophile and the chalcogen's region of positive electrostatic potential. Chalcogen bonding has been found to play an important role in various fields, mostly supramolecular catalysis, molecular recognition and crystal engineering [33–45].

Most investigations on chalcogen bonding involve divalent chalcogen atoms [33–45], although some report that ChBs in tetravalent sulfur compounds are also available in the literature [46]. It is well known that heavier elements have more intense σ-holes and

thus a higher tendency towards non-covalent and hypervalent binding [47]. In fact, in the case of tellurium (in practice, the heaviest element), it has multiple alternatives for self-organization that naturally lead to a higher tendency towards polymorphism [48,49]. This is typical for organotellurium halides, as shown by Turubaev et al. [50].

It has been reported that diorganyltellanes react with iodine to afford diiododiorganyltellurium(IV) [51,52]. In these molecules, the unique lone pair at Te is stereoactive; thus, it adopts a distorted trigonal bipyramid in which the three equatorial positions are occupied by organic groups and the lone pair, whereas the I atoms lie at the axial positions. In the solid state, these Te(IV) molecules generally show intermolecular chalcogen (Te···I) or halogen···halogen contacts I···I, with secondary bonding interactions leading to the formation of high-dimensional supramolecular frameworks (chains, layers or 3D networks) [53–64].

In this manuscript, a CSD (Cambridge Structural Database) [65] survey of the representative X-ray structures of $RR'TeI_2$ and $RTeI_3$ derivatives is provided to highlight the formation of Te···I ChBs (tellurium's σ-hole interacting with the negative belt at I) and I···I contacts (both type I and type II or HaBs) and also some atypical Te···I contacts where their definitions as ChB or HaB are not straightforward.

2. Results and Discussion

2.1. CSD Survey

In this section, which is not intended to be comprehensive, we have selected X-ray structures to illustrate the prevalence of the binding modes shown in Scheme 1.

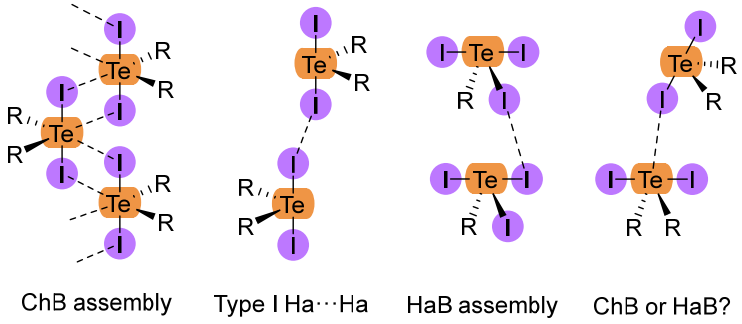

Scheme 1. Types of Te···I and I···I contacts analyzed in this work.

ChB Assemblies

Highly directional ChBs are observed in the solid state of most diiododiorganyltellurium(IV) X-ray structures deposited in the CSD. These ChBs govern the formation of either infinite 1D supramolecular chains or discrete 0D assemblies. As examples of structures exhibiting 1D assemblies, we have selected BZTELI10 [66], DIDMTE01 [64] and OPAXEJ [67], where supramolecular polymers propagate by means of the formation of quite directional ChBs. Each Te atom of one molecule establishes two Te···I ChBs with two adjacent molecules at distances that range from 3.696 to 3.955 Å, and they are clearly below the sum of van der Waals radii (ΣR_{vdW} = 4.2 Å) and above the sum of covalent radii (ΣR_{cov} = 2.77 Å). Moreover, the ChBs depicted in Figure 1 exhibit a strong directionality (C–Te···I angles close to 180°), thus suggesting that ChBs in the Te(IV) derivatives are more directional than in Te(II) systems [36]. It is interesting to highlight that the C–Te bond is pointing to the negative belt of I, thus suggesting that the I-atom is donating charge to the Te-atom, as further analyzed below. In dibenzotellurophene di-iodide (BZTELI10) and diethyl-diiodo-tellurium (OPAXEJ), both ChBs interactions are not identical (slightly different distances and angles), whilst for dimethyl-diiodo-tellurium (DIDMTE01), both ChBs are symmetrically equivalent. The existence of shorter ChB distances in BZTELI10 is likely due to the sp^2 nature of the C atoms bonded to Te that causes a greater polarization of the C–Te bond in comparison to the sp^3-hybridized C atoms of the other two compounds.

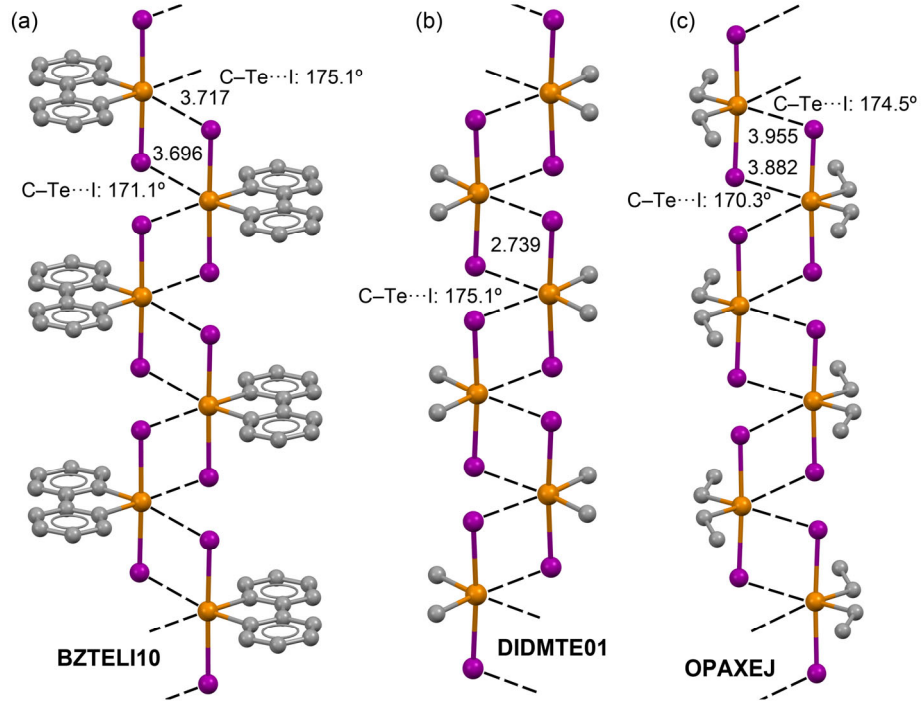

Figure 1. One-dimensional assemblies observed in the solid state of compounds BZTELI10 (**a**), DIDMTE01 (**b**) and OPAXEJ (**c**). H atoms not shown for clarity. Distances in Å. Color code: Carbon, grey; iodine, purple; tellurium, orange.

As an example of a 0D assembly, Figure 2 shows the X-ray structure of bis(4-methoxyphenyl)tellurium(IV) diiodide (NUNHUZ) [68]. Remarkably, the molecules are associated via directional ChBs with distances (3.692–3.902 Å) that are shorter than ΣR_{vdW}, and they form centrosymmetric tetramers in which the Te_4I_8 core displays a step-like geometry. The C–Te···I angles are quite linear apart from that of the longest contact (3.902 Å) where the angle is 158°.

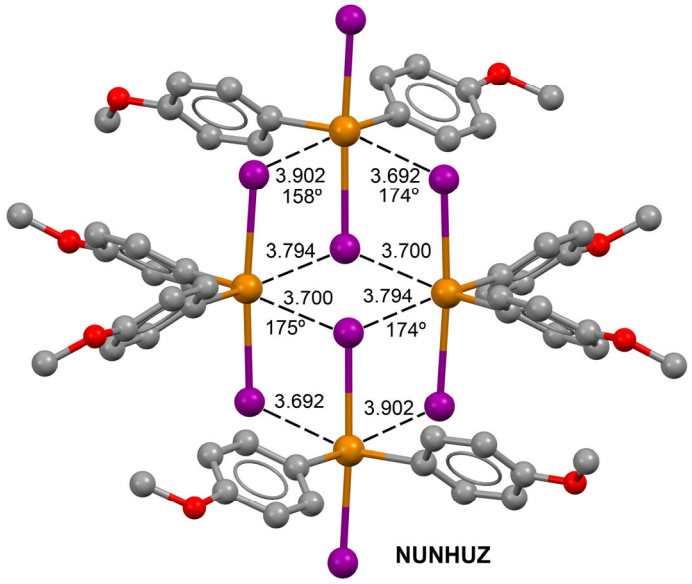

Figure 2. Centrosymmetric tetramer observed in the solid state of NUNHUZ. H atoms not shown for clarity. Distances in Å. Color code: oxygen in red; the rest are the same as in Figure 1.

Apart from the aforementioned tetrameric and 1D infinite assemblies, another concurrent motif in $RR'TeI_2$ compounds is the formation of self-assembled dimers. This occurs when an intramolecular ChB interaction blocks one of the σ-holes and, consequently, hampers supramolecular polymerization. Three illustrative examples are shown in Figure 3. The first one is (2-ethoxycyclohexyl)-tris(iodo)-tellurium (OPUXEF01) [50], presenting a short intramolecular Te···O contact involving the ethoxy O atom. A second example corresponds to 8-(diiodo(phenyl)-λ^4-tellanyl)-1-naphthyl phenyl sulfide (UKAFIW) [69] where the S atom in the peri-position establishes a short Te···S contact (3.077 Å) situated opposite to the Ph–Te bond. The third example [70] is similar to UKAFIW and corresponds to (6-(phenylsulfanyl)-1,2-dihydroacenaphthylen-5-yl)-diiodo-phenyl-tellurium, which also exhibits an intramolecular Te···S ChB (3.141 Å). In all three structures, short intermolecular contacts exist between the Te and I atoms of a neighboring molecule, generating a planar Te_2I_2 square (Figure 3). In all cases, the Te···I distances are shorter than ΣR_{vdW} for the two interacting atoms.

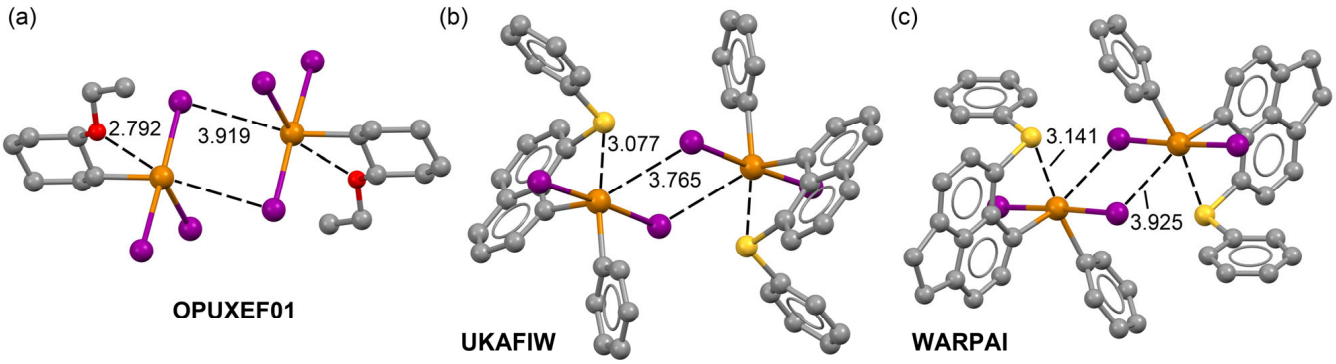

Figure 3. Self-assembled dimers observed in the solid state of compounds OPUXEF01 (**a**), UKAFIW (**b**) and WARPAI (**c**). H atoms not shown for clarity. Distances in Å. Color scheme: sulfur in yellow; the rest are the same as in Figure 1.

Apart from the ability of R_2TeI compounds to form 1D assemblies via ChBs, the tellurium triodides also have a marked tendency to form supramolecular polymers via halogen bonds (HaBs) instead of ChBs, where the σ-hole of one equatorial I atom interacts with the negative belt of one of the axial I atoms. Three examples are represented in Figure 4 to demonstrate this behavior. The first one is 2-biphenylyltellurium tri-iodide (BIPTEI01) [66], which exhibits a quite short I···I interaction (3.337 Å) taking into consideration that the ΣR_{vdW} of interacting atoms is 4.2 Å. One of the Te–I···I angles is close to 180°, and the other one close to 90°, which is compatible with the formation of a halogen bond that propagates the 2-biphenylyltellurium tri-iodide into the 1D polymer in the solid state (Figure 4a). Similarly, in (1-naphthyl)-tri-iodo-tellurium (MUWBIP) [71], short Te–I···I contacts govern the formation of 1D assemblies, with Te–I···I angles compatible with halogen-bonding interactions. Finally, the OPUXEF01 structure [50], also commented in the previous section, forms directional HaBs extending the 0D centrosymmetric dimers (planar Te_2I_2 square; see Figure 3a) to 1D assemblies. The I···I contacts depicted as dashed lines in Figure 4 are shorter than the Te···I contacts highlighted in Figures 1–3. Since the van der Waals radii of Te and I are the same (see Section 3), the shorter I···I distances suggest that HaBs are stronger than ChB, which is analyzed below.

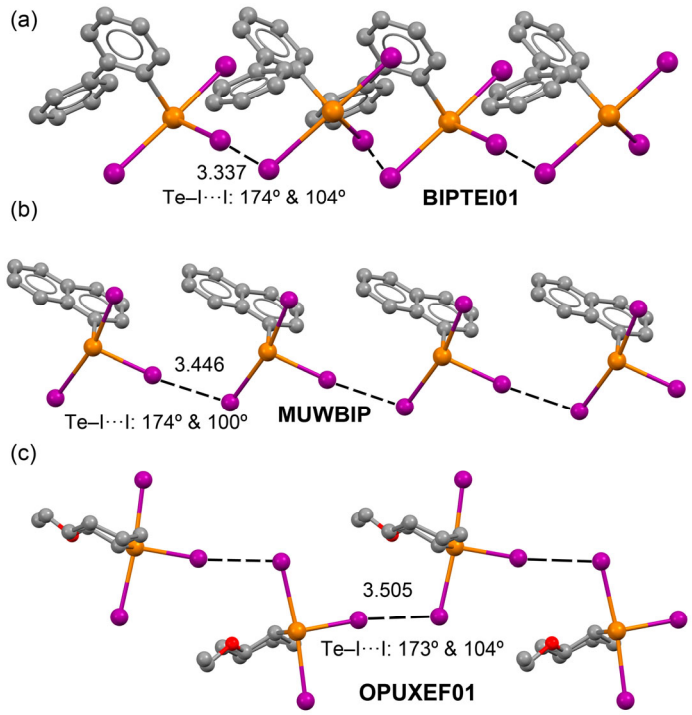

Figure 4. One-dimensional assemblies observed in the solid state of compounds BIPTEI01 (**a**), MUWBIP (**b**) and OPUXEF01 (**c**). H atoms not shown for clarity. Distances in Å. The color scheme is the same as in Figure 1.

Two categories of halogen···halogen contacts have been described in the literature, named type I and type II [72–74]. The examples of type II interactions are those of Figure 4 and fit the mold of a classic halogen bond [75–81], with one angle being 180° or thereabouts; thus, the σ-hole on one halogen atom can align with the negative region surrounding the other halogen when the second angle is roughly 90°. This orientation allows the lone pair of one halogen atom to line up with the σ* antibonding orbital facilitating the charge transfer. Type I geometry is characterized by interaction angles that are approximately equal to one another and generally within the vicinity of 140° or so. Intuitively, one would expect that the Type I interaction is destabilized relative to Type II due to the misalignments of the lone pairs and σ* orbitals of the interaction partners [82]. It has been proposed that structures with Type I interactions simply arise from close packing effects in the crystal [83–85]. Other explanations invoke anisotropic effects between elliptically shaped halogen atoms [86]; alternatively, they are controlled by dispersion [87]. The formation of the Type I I···I interaction is quite common in R_2TeI_2 compounds, as illustrated in Figure 5. For instance, the DIDMTE01 structure [64], also represented in Figure 1b, forms 1D chains with quite linear Te–I···I–Te contacts, identical Te–I···I angles (172.5°), and I···I distances that are significantly shorter than ΣR_{vdW}. Another example is shown in Figure 5b corresponding to bis(iodo)-(2-thienyl)-(trimethylsilylmethyl)-tellurium(IV) (ISALIY) [88], where the 1D assembly is propagated by Te–I···I–Te contacts with slightly different Te–I···I angles (169.0° and 170.5°) and parallel orientation of the monomers. Finally, Figure 5c shows the structure of 1-thia-4-tellura-cyclohexane 4,4-di-iodide (STEHEX) [89], which propagates in the solid state by means of Te–I···I–Te contacts with short I···I distances (3.663 Å) and slightly different Te–I···I angles (167.9° and 174.9°). It should be mentioned that, in general, the Te–I···I angles in the type I I···I interactions observed in R_2TeI_2 derivatives are closer to linearity (higher angles) than those observed in R–I···I–R Type I interactions that are usually close to 140°. The energy associated with this type of contact is discussed in the following sections.

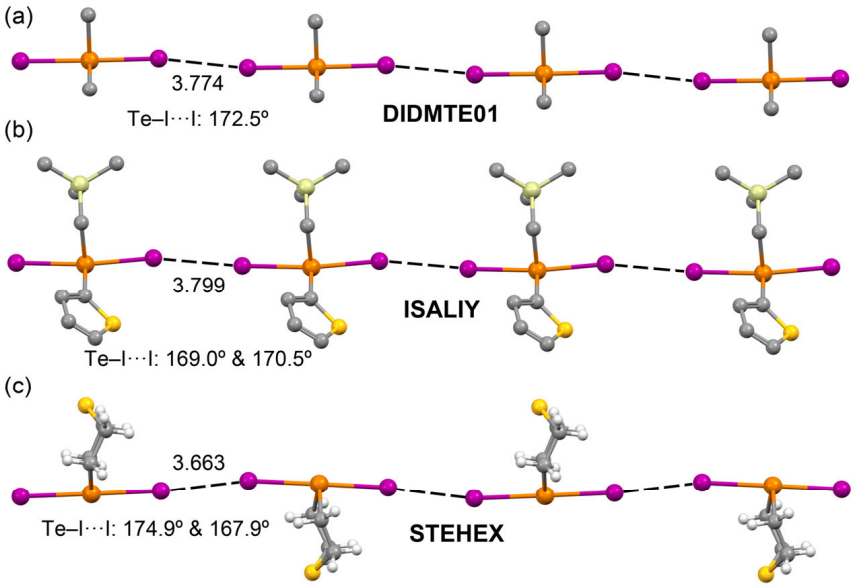

Figure 5. One-dimensional assemblies observed in the solid state of compounds DIDMTE01 (**a**), ISALIY (**b**) and STEHEX (**c**). H atoms not shown for clarity. Distances in Å. Color code: silicon in pale green; the rest are the same as in previous figures.

The inspection of the CSD also revealed some structures exhibiting Te···I contacts that are difficult to categorize; that is, structures that present short Te···I contacts with Te–I···Te angles that do not follow the expected geometry are considered as a σ-hole···σ-lump interaction. Three examples are gathered in Figure 6 with this characteristic binding model. In the case of triiodo-((Z)-2-chloro-1,2-diphenylvinyl)-tellurium(IV) (PEBHEN01) [90], the steroactive LP at Te points to the I-atom, consistent with the formation of an I···Te halogen bond. However, the Te–I···Te angle is not very linear (135.5°), which is not consistent with the formation of a halogen bond. The second example is 1-oxa-4-telluracyclohexane 4,4-di-iodide (OTEHEX) [91] where the interacting I-atom is indeed located opposite to one of the tellurium's σ-holes, but the Te–I···Te angle (156.8°) is not fully consistent with a ChB since the σ-hole is not pointing to the iodine's negative belt. A similar case of PEBHEN01 is also observed in (μ-η^5-cyclopentadienyl)-bis(η^5-cyclopentadienyl)-(1,3-dimethylimidazol-2-ylidene)-bis(iodo)-iron-nickel-tellurium (LOFCOB) [92]. More insights into these infringing Te···I contacts is provided in the theoretical section.

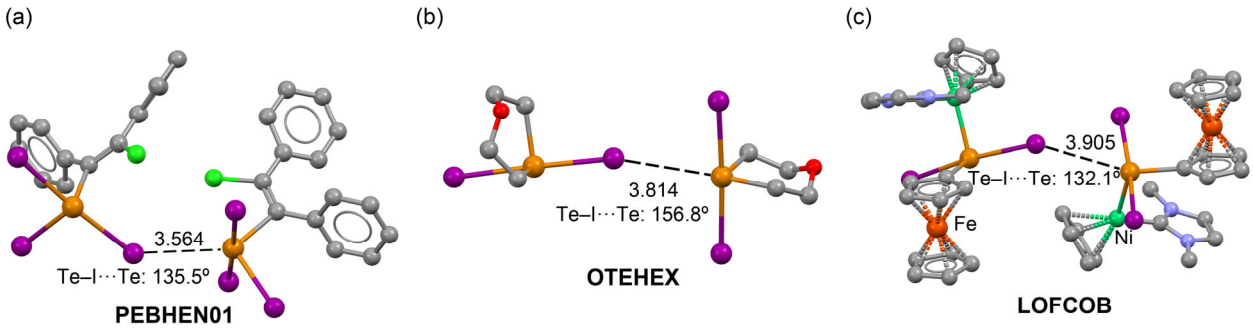

Figure 6. One-dimensional assemblies observed in the solid state of compounds PEBHEN01 (**a**), OTEHEX (**b**) and LOFCOB (**c**). H atoms not shown for clarity. Distances in Å. Color code: chlorine, green; nitrogen, blue; iron, dark orange; nickel, mint green; the rest are the same as in Figure 1.

2.2. Theoretical Study

2.2.1. C–Te···I ChBs

First, we analyzed a trimeric assembly of the BZTELI10 structure extracted from the 1D assembly represented in Figure 1a. Figure 7a shows the molecular electrostatic potential surface (MEP) of the monomer where it can be observed that the MEP maxima are located opposite to the C–Te bonds (37 kcal/mol) and the MEP minimum at the negative belt of the I-atom. This analysis strongly agrees with the formation of the directional C–Te···I ChBs in BZTELI10. It can be observed that the MEP value is also positive at the lone pair of Te (16 kcal/mol), and this is likely related to the inert lone pair effect. Finally, the MEP value at the iodine's σ-hole is a little negative (−6 kcal/mol), thus confirming the expected anisotropy at the iodine atom and that the axial iodine atoms are not good halogen bond donors. The combined "atoms in molecules" (AIM) and noncovalent interaction plot (NCIplot) analysis of the trimer is represented in Figure 7b. It can be observed that ChBs are characterized by a bond critical point (CP), bond path and a disk-shaped reduced density gradient (RDG) isosurface that connects Te to I atoms. The location of the I atom coincides with the MEP maximum, as shown in Figure 7a. The I atoms are also connected to the aromatic H atoms adjacent to the Te by a bond CP, bond path and green RDG isosurface, thus disclosing the existence of ancillary CH···I bonds. Finally, a bond CP and bond path connect one of the axial I atoms to one C atom of the aromatic dibenzotellurophene ring, thus revealing an I···π interaction. The formation energy of the assembly is substantial and negative (−17.26 kcal/mol), confirming the importance of such combinations of interactions in the solid state of BZTELI10. Orbital effects have been also analyzed using natural bond orbital (NBO) analysis since it is adequate for analyzing charge-transfer effects. Moreover, the second-order perturbation analysis can be used to obtain the stabilization energy due to the orbital charge transfer. The analysis and NBOs are gathered in Figure 7c. It can be observed that each ChB that is established in the trimer exhibits electron donations from a lone pair orbital (LP) at the iodine atom relative to the antibonding σ*(C–Te) orbital, thus confirming the σ hole chalcogen bonding nature of the interaction. The concomitant stabilization energy ($E^{(2)}$) values range from 8.2 to 10.0 kcal/mol, thus confirming the importance of LP(I)→σ*(C–Te) orbital effects.

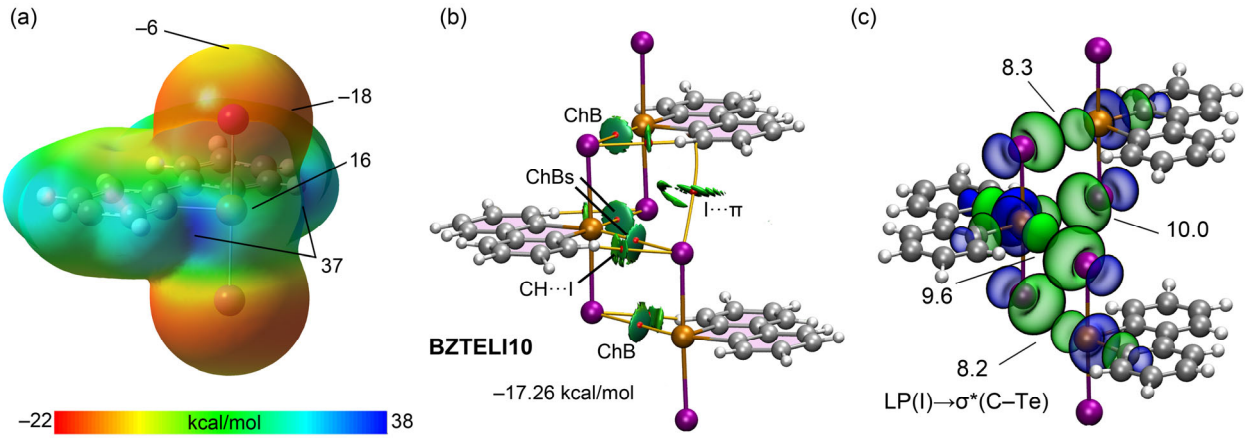

Figure 7. (**a**) MEP surface of BZTELI10 at the PBE0-D3/def2-TZVP level of theory. Energies in kcal/mol. (**b**) QTAIM (bond CPs in red and bond paths as orange lines) and NCIPlot (see theoretical methods for settings) analysis of BZTELI10. Only intermolecular contacts are shown. (**c**) NBOs and $E^{(2)}$ energies of donor–acceptor interactions in the trimeric assembly of BZTELI10. Energies in kcal/mol. Color code: See Figure 1.

Similar C–Te···I ChBs have also been analyzed in DIDMTE01, as shown in Figure 8. The MEP's surface analysis reveals the existence of two symmetric σ-holes at the Te atoms with an energy of 36 kcal/mol. The MEP minimum is located at the belt of the iodine atoms

(−14 kcal/mol). Similarly to the MEP obtained for BZTELI10, the iodine's σ-hole is very small and negative (−2 kcal/mol); therefore, establishing halogen-bonding interactions is not well suited. The plot in Figure 8b provides evidence that the ChBs in the trimer of DIDMTE01 are characterized by a bond critical point (CP), bond path and a bluish RDG isosurface that connects Te to the I atoms. One of the I atoms is also connected to one H atom of the methyl group of the adjacent molecule by a bond CP, bond path and green RDG isosurface, thus disclosing the existence of an ancillary CH···I bond. The formation energy of this assembly is moderately strong (−12.2 kcal/mol) and smaller than that of BZTELI10 because of the extra C_{sp2}–H···I H bonds in the latter. Similarly to BZTELI10, the NBO shows the existence of a relevant LP(I) →σ*(C–Te) charge transfer ($E^{(2)}$ = 6.0–6.8 kcal/mol), confirming the σ-hole nature of the contact.

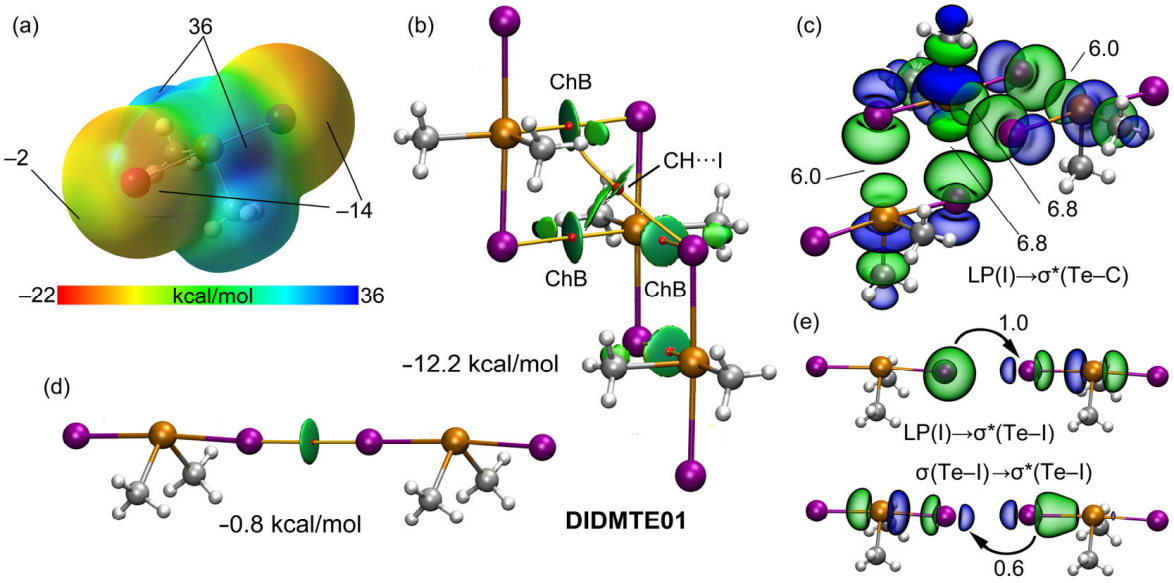

Figure 8. (**a**) MEP surface of the DIDMTE01 monomer at the PBE0-D3/def2-TZVP level of theory. Energies in kcal/mol. (**b**) QTAIM (bond CPs in red and bond paths as orange lines) and NCIplot (see theoretical methods for settings) analysis of a trimer of DIDMTE01. Only intermolecular contacts are shown. (**c**) NBOs and $E^{(2)}$ energies of the donor–acceptor interactions in the trimeric assembly of DIDMTE01. Energies in kcal/mol. (**d**) QTAIM (bond CPs in red and bond paths as orange lines) and NCIplot (see theoretical methods for settings) analysis of a dimer of DIDMTE01. (**e**) NBOs and $E^{(2)}$ energies of the donor–acceptor interactions in the dimeric assembly of DIDMTE01. Energies in kcal/mol. Color code: See Figure 1.

2.2.2. Te–I···I–Te Type I Halogen···Halogen Interactions

As commented above in Figure 5, several R_2TeI derivatives exhibit type I I···I interactions, leading to the formation of infinite 1D chains. This type of interaction is characterized by two large and similar Te–I···I angles. In the case of the DIDMTE01 structure, both angles are identical (172.5°; see Figure 5a). This angle is larger than the angle reported in typical EWG–I···I–EWG type I interactions [82]. This is likely due to the negligible MEP value at the prolongation of the Te–I bond (−2 kcal/mol; see Figure 8a), thus reducing the electrostatic repulsion. The QTAIM/NCIplot analysis of the DIDMTE01 shows a bond CP and bond path interconnecting the I atoms. Moreover, the type I interaction is also revealed by a disk-shaped green RDG isosurface located coincidently to the bond CP. The interaction energy is very small (−0.8 kcal/mol), as is usual in this type of contact [82]. The NBO analysis (see Figure 8e) shows two types of orbital donor–acceptor contributions. One contribution is from the LP at one iodine to the antibonding σ*(Te–I), and the other contribution is from the bonding σ(Te–I) orbital of one unit to the antibonding σ*(Te–I) orbital of the other unit. The total stabilization due to the charge transfer is $E^{(2)}$ = 1.6 kcal/mol.

This type of interaction has also been studied in the OPAXEJ structure that forms discrete dimers instead of 1D infinite chains in the solid state. The MEP surface of OPAXEJ is shown in Figure 9, evidencing the existence of σ-holes (MEP maxima, 30 kcal/mol). The MEP minimum is located at the iodine's negative belt (−16 kcal/mol) and the MEP value at the σ-hole of iodine is −2 kcal/mol. In this type I halogen···halogen dimer, the Te–I···I angles are identical (154.2°), and they are quite smaller than those in the DIDMTE01 structure. This explains the slightly larger interaction energy (−1.0 kcal/mol) due to the smaller electrostatic repulsion. However, in this structure, the charge transfer is almost negligible (0.5 kcal/mol). It emerges from an electron donation LP at one iodine to the antibonding σ*(Te–I), as shown in Figure 9c.

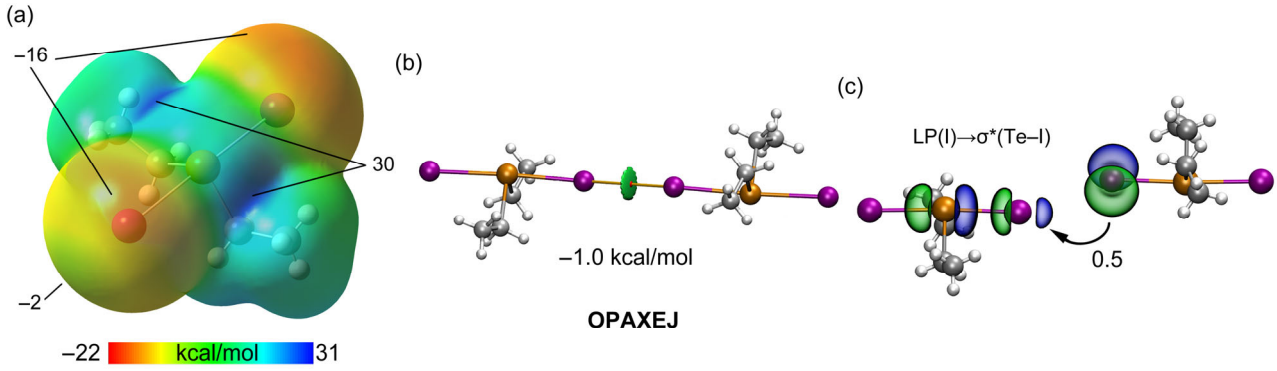

Figure 9. (**a**) MEP surface of the OPAXEJ monomer at the PBE0-D3/def2-TZVP level of theory. Energies in kcal/mol. (**b**) QTAIM (bond CPs in red and bond paths as orange lines) and NCIplot (see theoretical methods for settings) analysis of a dimer of OPAXEJ. Only intermolecular contacts are shown. (**c**) NBOs and $E^{(2)}$ energies of the donor–acceptor interactions in the dimer of OPAXEJ. Energies in kcal/mol. Color code: See Figure 1.

2.2.3. Te–I···I–Te Halogen-Bonding Interactions

As detailed in Figure 4 (*vide supra*), some triiodide derivatives ($RTeI_3$) also form HaB assemblies in the solid state. One of them (OPUXEF) has been studied theoretically. Interestingly, the MEP surface analysis (Figure 10a) shows that the equatorial iodine atom exhibits a large and positive σ-hole (+18 kcal/mol) in contrast to the behavior of the axial iodine atoms that present either negative (−11 kcal/mol) or electroneutral (0 kcal/mol) MEP values. The MEPs at the negative belts of the axial iodine atoms are −22 and −9 kcal/mol. The QTAIM/NCIplot analysis of the HaB dimer shows that the equatorial I atom is connected to one of the axial I atoms by a bond CP, bond path and blue RDG isosurface, indicating a strong and attractive HaB. An extra bond CP, bond path and green RDG isosurface also interconnect two additional I atoms. Such contact is likely due to weak van der Waals forces and the spatial proximity of both atoms. The green RDG isosurface also embraces part of the Te atom, thus also suggesting some Te···I interactions. The dimerization energy is moderately strong (−8.7 kcal/mol), in line with the blue RDG isosurface. In comparison to the binding energies of the ChB assemblies shown in Figures 7b and 8b (−17.26 kcal/mol and −12.2 kcal/mol) where four ChBs were established, the binding energy of the HaB dimer of Figure 10b, where only one HaB is formed, provides evidence that the HaB is stronger than the ChB, in line with the shorter HaB distances observed in X-ray structures (vide supra) in comparison to ChB distances. The NBO analysis is very useful for shedding light on the nature of different contacts, which is represented in Figure 10c. The HaB nature of Te–I···I is confirmed since the typical LP(I)→σ*(Te–I) electron transfer is found with a concomitant stabilization energy of $E^{(2)}$ = 11.0 kcal/mol, thus evidencing the dominant role of the HaB. There is a secondary charge transfer from an LP at the axial I atom to the antibonding σ*(Te–C) orbital, thus disclosing a weak ChB interaction at $E^{(2)}$ = 1.3 kcal/mol.

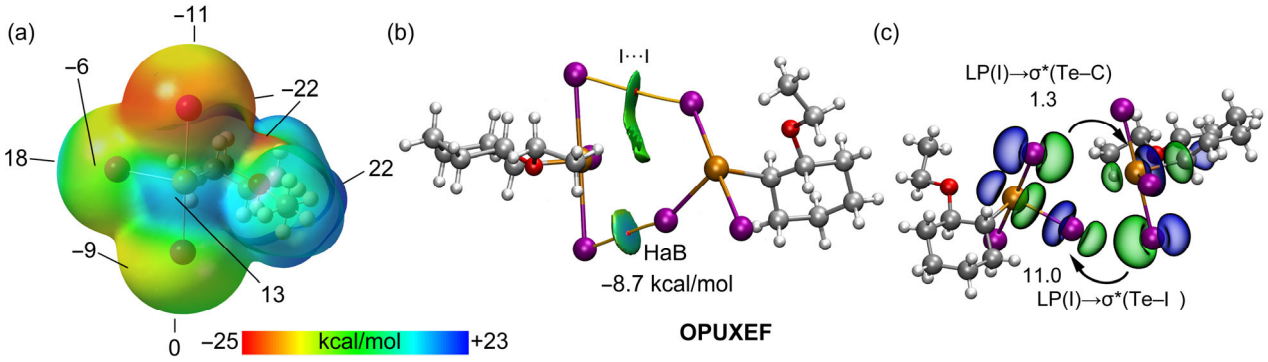

Figure 10. (**a**) MEP surface of the OPUXEF monomer at the PBE0-D3/def2-TZVP level of theory. Energies in kcal/mol. (**b**) QTAIM (bond CPs in red and bond paths as orange lines) and NCIplot (see theoretical methods for settings) analysis of a dimer of OPUXEF. Only intermolecular contacts are shown. (**c**) NBOs and $E^{(2)}$ energies of the donor–acceptor interactions in the dimer of OPUXEF. Energies in kcal/mol. Color code: See Figure 1.

2.2.4. Uncategorized Te···I Contacts

As discussed above, some Te···I contacts observed in the X-ray structures gathered in Figure 6 were difficult to categorize. For example, in PEBHEN01, the LP at Te is pointing to the I atom, consistent with the formation of an I···Te halogen bond (Figure 11). However, the MEP surface analysis shows that the MEP value is positive at the LP of the Te atom (+22 kcal/mol) and negative at the axial I atoms (ranging from −19 kcal/mol at the belt to −3 kcal/mol at the σ-hole), which is more consistent with a ChB. The QTAIM analysis confirms the existence of the Te···I contact characterized by the corresponding bond CP, bond path and bluish RDG isosurface. The analysis also discloses the presence of several ancillary interactions, characterized by bond CPs, bond paths and green RDG isosurfaces (CH···π, Cl···π and Cl···I). Indeed, the MEP surface shows a σ-hole at the Cl-atom (16 kcal/mol), which is consistent with the formation of a Cl···π interaction. Moreover, the MEP value at the aromatic H atoms is also large and positive (+20 kcal/mol), which is also consistent with the formation of CH···π interactions. Such combinations of interactions explain the large interaction energy of −9.3 kcal/mol. Finally, the NBO confirms the ChB nature of the interaction, since an LP(I)→σ*(Te–C) electron transfer is observed to exhibit a significant stabilization energy of $E^{(2)}$ = 4.1 kcal/mol.

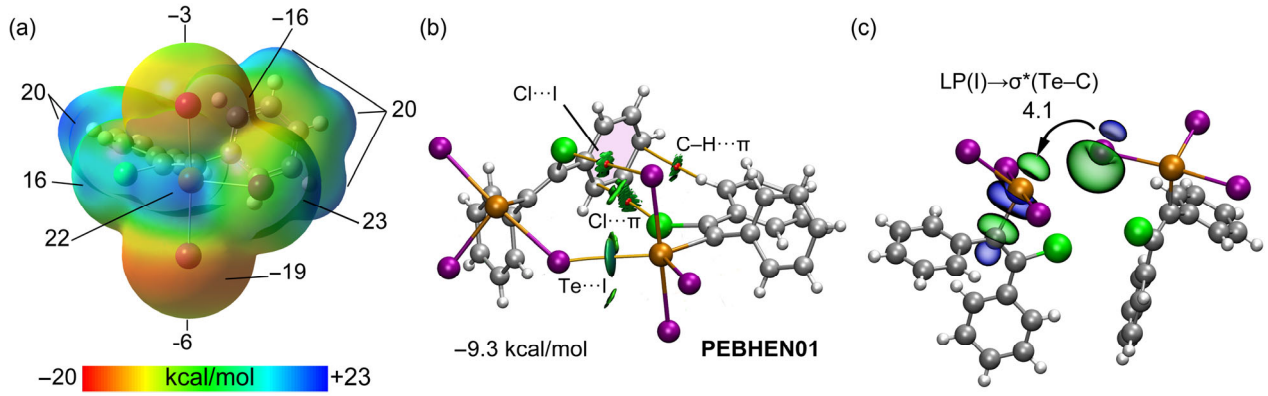

Figure 11. (**a**) MEP surface of a PEBHEN01 monomer at the PBE0-D3/def2-TZVP level of theory. Energies in kcal/mol. (**b**) QTAIM (bond CPs in red and bond paths as orange lines) and NCIplot (see theoretical methods for settings) analysis of a dimer of PEBHEN01. Only intermolecular contacts are shown. (**c**) NBOs and $E^{(2)}$ energies of the donor–acceptor interactions in the dimer of PEBHEN01. Energies in kcal/mol. Color code: Refer to previous figures.

A second example has been analyzed that corresponds to the OTEHEX structure (Figure 12), where the interacting I atom is located opposite to one of the tellurium's σ-holes, but the Te–I···Te angle (156.8°) is not fully consistent with a ChB, since the σ-hole is not pointing directly to the iodine's negative belt (see Figure 6b above). The MEP surface shown in Figure 12a reveals that the MEP maximum is located at the σ-holes of the tellurium atom (+30 kcal/mol) and that the MEP is negative at the I atom (−15 kcal/mol at the belt and −3 kcal/mol at the σ-hole). This MEP analysis anticipates the ChB nature of interactions. The combined QTAIM/NCIplot analysis confirms the interaction by means of a bond CP, bond path and a greenish RDG isosurface. The latter extends to the region between both I atoms, thus suggesting some I···I van der Waals contact. The interaction energy is modest (−2.7 kcal/mol) and in line with the unideal directionality of the interaction. The NBO corroborates the ChB nature of the interaction, disclosing an LP(I)→σ*(Te–C) electron transfer with a modest stabilization energy of $E^{(2)}$ = 1.6 kcal/mol.

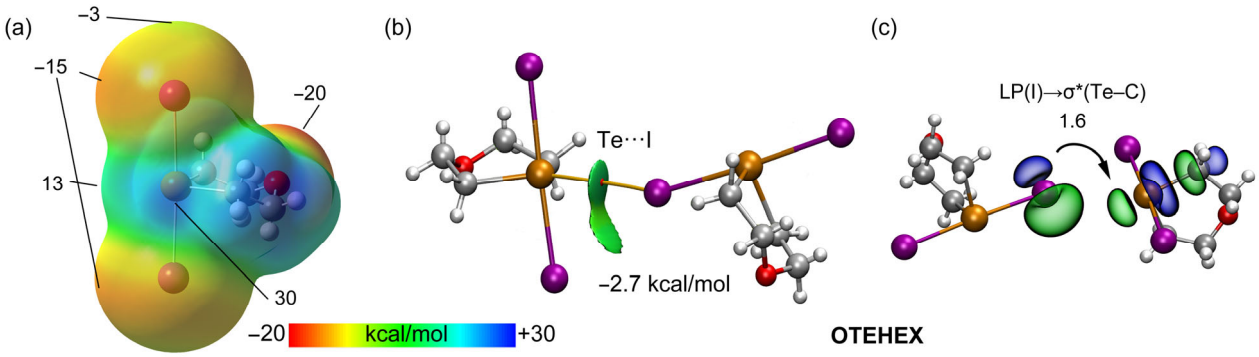

Figure 12. (**a**) MEP surface of the OTEHEX monomer at the PBE0-D3/def2-TZVP level of theory. Energies in kcal/mol. (**b**) QTAIM (bond CPs in red and bond paths as orange lines) and NCIplot (see theoretical methods for settings) analysis of a dimer of OTEHEX. Only intermolecular contacts are shown. (**c**) NBOs and $E^{(2)}$ energies of the donor–acceptor interactions in the dimer of OTEHEX. Energies in kcal/mol. Color code: See Figure 1.

2.2.5. Energy Decomposition Analysis

The Kitaura–Morokuma decomposition analysis (see computational methods) has been applied to the assemblies analyzed in Figures 7–12 to investigate the relative importance of exchange repulsion ($E_{ex\text{-}rep}$), electrostatic (E_{el}), correlation (E_{cor}), dispersion (E_{disp}) and orbital (E_{orb}) terms for different interactions (ChB, HaB and type I I···I). The results are summarized in Figure 13, and they show that the electrostatic force is the most important attractive component in the ChB assemblies of BZTELI10 and DIDMTE01, which is in line with the MEP analysis, since the Te···I contact involves atoms with the maximum and minimum MEP values with the expected directionality. The second major attractive force is the orbital component, which is also in line with the large stabilization energies provided by the NBO analysis (see Figures 7, 8 and 10). Finally, the correlation and dispersion terms are also significant in both BZTELI10 and DIDMTE01 ChB assemblies. In the case of type I interactions (DIDMTE01 and OPAXEJ), the behavior is different since the orbital term is the most important followed by the correlation. Dispersion and electrostatic forces are the weakest forces for these types of systems. For the halogen-bonded assembly, the main component is electrostatic forces followed by the orbital term, which is also in agreement with the MEP and NBO analyses of Figure 10, and parallel to the ChB interactions in the BZTELI10 and DIDMTE01 structures. It is interesting to highlight that in the ChB assembly of OTEHEX with a poor C–Te···I–Te directionality, all attractive terms are similar, ranging from −2.2 kcal/mol for dispersion to −3.0 kcal/mol for the correlation. In the case of PEBHEN01, again with a poor C–Te···I–Te directionality, the ChB is not dominated by the electrostatic contribution, as observed in the directional ChBs in BZTELI10 and DIDMTE01 structures. Conversely, it is dominated by the orbital, followed by dispersion contributions.

This is the only structure where dispersion is very relevant, which is due to the participation of the aromatic ring in several contacts, as detailed in Figure 11b.

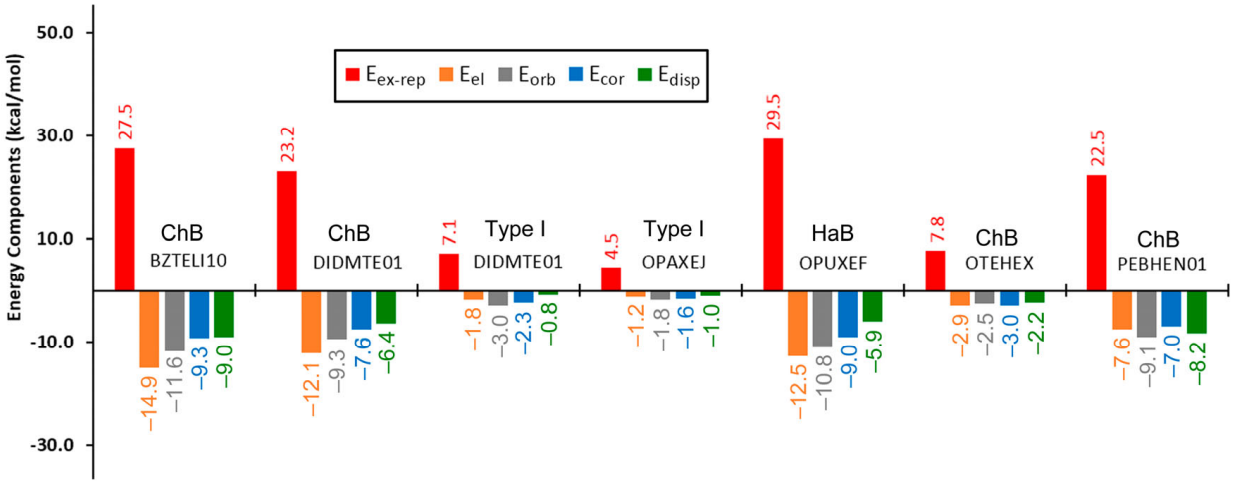

Figure 13. Exchange–repulsion ($E_{ex\text{-}rep}$), electrostatic (E_{el}), correlation (E_{cor}), dispersion (E_{disp}) and orbital (E_{orb}) energetic terms for the assemblies of Figures 7–12 in kcal/mol using the Kitaura–Morokuma analysis.

3. Computational Methods

The calculations were performed using Turbomole program 7.7 [93] at the PBE0-D3/def2-TZVP level of theory [94–97]. The MEP surfaces were plotted using the 0.001 a.u. isosurface. The QTAIM [98] and NCIPlot [99] analyses were represented using VMD software [100]. The Multiwfn program [101] was used for QTAIM and NCIplot calculations. The following settings were used to represent the NCIplot in the figures of this manuscript: RDG = 0.5; ρ cut-off = 0.04 a.u.; color code -0.035 a.u. $\leq$ (signλ_2)$\rho \leq 0.035$ a.u. Natural bond orbital (NBO) analysis [102] was performed using the NBO7 program [103]. The EDA analysis was performed using the Kitaura–Morokuma method [104], as implemented in Turbomole 7.7 without a basis set superposition error (BSSE) correction. In this manuscript, the van der Waals radii proposed by Batsanov have been used (2.1 Å, for Te and I) [105]. For calculations, we have used X-ray coordinates (see Supplementary Materials) because we are interested in evaluating and characterizing the interactions as they stand in the solid state. The level of theory used in this work (both the DFT method and basis set) has been previously used to analyze halogen- and chalcogen-bonding interactions [106–112] and also demonstrated that the interaction energies are comparable to those using state-of-the-art CCSD(T)/CBS calculations [16].

4. Conclusions

The formation of several recurrent motifs in R_2TeI_2 and $RTeI_3$ derivatives was analyzed by examining the CSD and using DFT calculations. For R_2TeI_2 molecules, the prevalence of ChBs was observed, leading to the formation of 1D polymers or self-assembled dimers in the solid state. Moreover, the formation of type I I···I contacts was also common. Such interactions are weak (around 1 kcal/mol) and dominated by orbital and correlation forces. In the case of $RTeI_3$ derivatives, the equatorial I atom exhibits a positive σ-hole; thus, it is adequate for establishing HaB assemblies. Both directional ChBs and HaBs are dominated by electrostatic effects, followed by the orbital contribution, and this is in line with MEP and NBO analyses. Finally, some structures also exhibit some poorly directional ChBs that have been characterized by QTAIM, NBO and EDA analyses. In these assemblies, the electrostatic force is not the main component (due to the poor directionality), and other components such as the orbital, correlation or dispersion terms are more dominant.

Supplementary Materials: The following supporting information can be downloaded at https://www.mdpi.com/article/10.3390/inorganics11050209/s1, Cartesian coordinates of the compounds and their assemblies.

Author Contributions: Conceptualization, A.B. and A.F.; methodology, R.M.G. and S.B.; software, R.M.G. and S.B.; validation, A.B. and A.F.; formal analysis, R.M.G. and S.B.; investigation, R.M.G. and S.B.; writing—original draft preparation, A.F.; writing—review and editing, A.B., A.F., R.M.G. and S.B.; supervision, A.F.; project administration, A.F.; funding acquisition, A.F. All authors have read and agreed to the published version of the manuscript.

Funding: This research was funded by the "Ministerio de Ciencia, Innovación y Universidades" and "Agencia Estatal de Investigacion" (MICIU/AEI) of Spain (project PID2020-115637GB-I00 FEDER funds).

Data Availability Statement: No new data were created.

Acknowledgments: The "centre de technologies de la informació" (CTI) is gratefully acknowledged for their computational facilities.

Conflicts of Interest: The authors declare no conflict of interest.

References

1. Desiraju, G.R.; Ho, P.S.; Kloo, L.; Legon, A.C.; Marquardt, R.; Metrangolo, P.; Politzer, P.; Resnati, G.; Rissanen, K. Definition of the halogen bond (IUPAC Recommendations 2013). *Pure Appl. Chem.* **2013**, *85*, 1711–1713. [CrossRef]
2. Aakeroy, C.B.; Bryce, D.L.; Desiraju, G.R.; Frontera, A.; Legon, A.C.; Nicotra, F.; Rissanen, K.; Scheiner, S.; Terraneo, G.; Metrangolo, P.; et al. Definition of the chalcogen bond (IUPAC Recommendations 2019). *Pure Appl. Chem.* **2019**, *91*, 1889–1892. [CrossRef]
3. Zahn, S.; Frank, R.; Hey-Hawkins, E.; Kirchner, B. Pnicogen bonds: A new molecular linker? *Chem. Eur. J.* **2011**, *17*, 6034–6038. [CrossRef]
4. Bauzá, A.; Mooibroek, T.J.; Frontera, A. Tetrel Bonding Interaction: Rediscovered Supramolecular Force? *Angew. Chem. Int. Ed.* **2013**, *52*, 12317–12321. [CrossRef] [PubMed]
5. Bauzá, A.; Frontera, A. σ/π-Hole noble gas bonding interactions: Insights from theory and experiment. *Coord. Chem. Rev.* **2020**, *404*, 213112. [CrossRef]
6. Bauzá, A.; Frontera, A.; Mooibroek, T.J. NO_3^- anions can act as Lewis acid in the solid state. *Nat. Commun.* **2017**, *8*, 14522. [CrossRef]
7. García-Llinás, X.; Bauzá, A.; Seth, S.K.; Frontera, A. Importance of R–CF_3···O Tetrel Bonding Interactions in Biological Systems. *J. Phys. Chem. A* **2017**, *28*, 5371–5376. [CrossRef]
8. Bauzá, A.; Sharko, A.V.; Senchyk, G.A.; Rusanov, E.B.; Frontera, A.; Domasevitch, K.V. π–hole interactions at work: Crystal engineering with nitro-derivatives. *Cryst. Eng. Comm.* **2017**, *19*, 1933–1937. [CrossRef]
9. Bauzá, A.; Frontera, A.; Mooibroek, T.J. π-hole interactions involving nitro compounds: Directionality of nitrate esters. *Cryst. Growth Des.* **2016**, *16*, 5520–5524. [CrossRef]
10. Politzer, P.; Murray, J. σ-Hole Interactions: Perspectives and Misconceptions. *Crystals* **2017**, *7*, 212. [CrossRef]
11. Politzer, P.; Murray, J.S.; Clark, T. Halogen bonding and other σ-hole interactions: A perspective. *Phys. Chem. Chem. Phys.* **2013**, *15*, 11178–11189. [CrossRef] [PubMed]
12. Bauza, A.; Mooibroek, T.J.; Frontera, A. The Bright Future of Unconventional σ/π-Hole Interactions. *Chem. Phys. Chem.* **2015**, *16*, 2496–2517. [CrossRef]
13. Riwar, L.J.; Trapp, N.; Root, K.; Zenobi, R.; Diederich, F. Supramolecular Capsules: Strong versus Weak Chalcogen Bonding. *Angew. Chem. Int. Ed.* **2018**, *57*, 17259–17264. [CrossRef] [PubMed]
14. Wonner, P.; Dreger, A.; Vogel, L.; Engelage, E.; Huber, S.M. Chalcogen Bonding Catalysis of a Nitro-Michael Reaction. *Angew. Chem. Int. Ed.* **2019**, *58*, 16923–16927. [CrossRef]
15. Borissov, A.; Marques, I.; Lim, J.Y.C.; Félix, V.; Smith, M.D.; Beer, P.D. Anion Recognition in Water by Charge-Neutral Halogen and Chalcogen Bonding Foldamer Receptors. *J. Am. Chem. Soc.* **2019**, *141*, 4119–4129. [CrossRef]
16. Mallada, B.; Gallardo, A.; Lamanec, M.; De La Torre, B.; Špirko, V.; Hobza, P.; Jelinek, P. Real-space imaging of anisotropic charge of σ-hole by means of Kelvin probe force microscopy. *Science* **2021**, *374*, 863–867. [CrossRef]
17. Pascoe, J.; Ling, K.B.; Cockroft, S.L. The Origin of Chalcogen-Bonding Interactions. *J. Am. Chem. Soc.* **2017**, *139*, 15160–15167. [CrossRef]
18. Macchione, M.; Goujon, A.; Strakova, K.; Humeniuk, H.V.; Licari, G.; Tajkhorshid, E.; Sakai, N.; Matile, S. A Chalcogen-Bonding Cascade Switch for Planarizable Push-Pull Probes. *Angew. Chem. Int. Ed.* **2019**, *58*, 15752–15756. [CrossRef]
19. Politzer, P.; Murray, J.S. An overview of strengths and directionalities of noncovalent interactions: σ-holes and π-holes. *Crystals* **2019**, *9*, 165. [CrossRef]
20. Politzer, P.; Murray, J.S.; Clark, T.; Resnati, G. The σ-hole revisited. *Phys. Chem. Chem. Phys.* **2017**, *19*, 32166–32178. [CrossRef] [PubMed]

21. Murray, J.S.; Lane, P.; Clark, T.; Riley, K.E.; Politzer, P. σ-Holes, π-holes and electrostatically-driven interactions. *J. Mol. Mod.* **2012**, *18*, 541–548. [CrossRef] [PubMed]
22. Cavallo, G.; Metrangolo, P.; Pilati, T.; Resnati, G.; Terraneo, G. Naming interactions from the electrophilic site. *Cryst. Growth Des.* **2014**, *14*, 2697–2702. [CrossRef]
23. Terraneo, G.; Resnati, G. Bonding Matters. *Cryst. Growth Des.* **2017**, *17*, 1439–1440. [CrossRef]
24. Scheiner, S. Steric crowding in tetrel bonds. *J. Phys. Chem. A* **2018**, *122*, 2550–2562. [CrossRef]
25. Bauzá, A.; Mooibroek, T.J.; Frontera, A. Tetrel Bonding Interactions. *Chem. Rec.* **2016**, *16*, 473–487. [CrossRef] [PubMed]
26. Mani, D.; Arunan, E. The X–C· · · Y (X = O/F, Y = O/S/F/Cl/Br/N/P) 'carbon bond' and hydrophobic interactions. *Phys. Chem. Chem. Phys.* **2013**, *15*, 14377–14383. [CrossRef]
27. Sethio, D.; Oliveira, V.; Kraka, E. Quantitative Assessment of Tetrel Bonding Utilizing Vibrational Spectroscopy. *Molecules* **2018**, *23*, 2763. [CrossRef]
28. Heywood, V.L.; Alford, T.P.J.; Roeleveld, J.J.; Deprez, S.J.L.; Verhoofstad, A.; van der Vlugt, J.I.; Domingos, S.R.; Schnell, M.; Davis, A.P.; Mooibroek, T.J. Observations of tetrel bonding between sp3-carbon and THF. *Chem. Sci.* **2020**, *11*, 5289–5293. [CrossRef]
29. Zhang, Y.; Wang, W.; Wang, Y.-B. Tetrel bonding on Graphene. *Comp. Theor. Chem.* **2019**, *1147*, 8–12. [CrossRef]
30. Taylor, M.S. Anion recognition based on halogen, chalcogen, pnictogen and tetrel bonding. *Coord. Chem. Rev.* **2020**, *413*, 213720. [CrossRef]
31. Bauzá, A.; Seth, S.K.; Frontera, A. Tetrel bonding interactions at work: Impact on tin and lead coordination compounds. *Coord. Chem. Rev.* **2019**, *384*, 107–125. [CrossRef]
32. Mundlapati, V.R.; Sahoo, D.K.; Bhaumik, S.; Jena, S.; Chandrakar, A.; Biswal, H.S. Noncovalent Carbon-Bonding Interactions in Proteins. *Angew. Chem. Int. Ed.* **2018**, *57*, 16496. [CrossRef] [PubMed]
33. Scilabra, P.; Terraneo, G.; Resnati, G. The Chalcogen Bond in Crystalline Solids: A World Parallel to Halogen Bond. *Acc. Chem. Res.* **2019**, *52*, 1313–1324. [CrossRef] [PubMed]
34. Fourmigué, M.; Dhaka, A. Chalcogen bonding in crystalline diselenides and selenocyanates: From molecules of pharmaceutical interest to conducting materials. *Coord. Chem. Rev.* **2020**, *403*, 213084. [CrossRef]
35. Alkorta, I.; Elguero, J.; Frontera, A. Not only hydrogen bonds: Other noncovalent interactions. *Crystals* **2020**, *10*, 180. [CrossRef]
36. Vogel, L.; Wonner, P.; Huber, S.M. Chalcogen bonding: An overview. *Angew. Chem. Int. Ed.* **2019**, *58*, 1880–1891. [CrossRef] [PubMed]
37. Biot, N.; Bonifazi, D. Chalcogen-bond driven molecular recognition at work. *Coord. Chem. Rev.* **2020**, *413*, 213243. [CrossRef]
38. Navarro-García, E.; Galmés, B.; Velasco, M.D.; Frontera, A.; Caballero, A. Anion Recognition by Neutral Chalcogen Bonding Receptors: Experimental and Theoretical Investigations. *Chem. Eur. J.* **2020**, *26*, 4706–4713. [CrossRef] [PubMed]
39. Navarro-García, E.; Galmés, B.; Velasco, M.D.; Bastida, A.; Zapata, F.; Caballero, A.; Frontera, A. Host–guest complexes vs. supramolecular polymers in chalcogen bonding receptors: An experimental and theoretical study. *Dalton Trans.* **2022**, *51*, 1325–1332. [CrossRef]
40. Frontera, A.; Bauza, A. Metal Coordination Enhances Chalcogen Bonds: CSD Survey and Theoretical Calculations. *Int. J. Mol. Sci.* **2022**, *23*, 4188. [CrossRef]
41. Mahmudov, K.T.; Kopylovich, M.N.; Guedes da Silva, M.F.C.; Pombeiro, A.J.L. Chalcogen bonding in synthesis, catalysis and design of materials. *Dalton Trans.* **2017**, *46*, 10121–10138. [CrossRef] [PubMed]
42. Romito, D.; Fresta, E.; Cavinato, L.M.; Kählig, H.; Amenitsch, H.; Caputo, L.; Chen, Y.; Samorì, P.; Charlier, J.-C.; Costa, R.D.; et al. Supramolecular Chalcogen-Bonded Semiconducting Nanoribbons at Work in Lighting Devices. *Angew. Chem. Int. Ed.* **2022**, *61*, e202202137. [CrossRef] [PubMed]
43. Adhikari, U.; Scheiner, S. Effects of Charge and Substituent on the S···N Chalcogen Bond. *J. Phys. Chem. A* **2014**, *118*, 3183–3192. [CrossRef]
44. Goodman, M.A.; Detty, M.R. Selenoxides as Catalysts for the Activation of Hydrogen Peroxide. Bromination of Organic Substrates with Sodium Bromide and Hydrogen Peroxide. *Organometallics* **2004**, *23*, 3016–3020. [CrossRef]
45. Farina, M.; Folmer, V.; Bolzan, R.C.; Andrade, L.H.; Zeni, G.; Braga, A.J.; Rocha, J.B.T. Selenoxides inhibit δ-aminolevulinic acid dehydratase. *Toxicol. Lett.* **2001**, *119*, 27–37. [CrossRef]
46. Franconetti, A.; Quiñonero, D.; Frontera, A.; Resnati, G. Unexpected chalcogen bonds in tetravalent sulfur compounds. *Phys. Chem. Chem. Phys.* **2019**, *21*, 11313–11319. [CrossRef] [PubMed]
47. Alcock, N.W.; Harrison, W.D. Secondary bonding. Part 12. Aryltellurium iodides: Crystal and molecular structures of cis- and trans-phenyltellurium(IV) tri-iodide and two modifications of diphenyltellurium(IV) di-iodide. *J. Chem. Soc. Dalton Trans.* **1984**, 869–875. [CrossRef]
48. Raatikainen, K.; Rissanen, K. Hierarchical halogen bonding induces polymorphism. *CrystEngComm* **2009**, *11*, 750–752. [CrossRef]
49. Haddad, S.F.; Willett, R.D.; Twamley, B. The Role of Hydrogen Bonding and Halogen Bonding in the Polymorphic Structures of 3,5-Dibromo-2,6-diaminopyridinium Bromide. *J. Chem. Crystallogr.* **2010**, *40*, 902–908. [CrossRef]
50. Torubaev, Y.V.; Skabitsky, I.V. Crystals at a Carrefour on the Way through the Phase Space: A Middle Path. *Molecules* **2021**, *26*, 1583. [CrossRef]
51. Hargittai, J.; Rozsondai, B. *The Chemistry of Organic Selenium and Tellurium Compounds*; Patai, S., Rappoport, Z., Eds.; Wiley: New York, NY, USA, 1986; Volume 1, p. 63.

52. Lrgolic, K.J. *Synthetic Methods of Organometallic and Inorganic Chemistry*; Herrmann, W.A., Cybill, C.E., Eds.; Georg Thieme Verlag: New York, NY, USA, 1997; Volume 4, p. 219.
53. Närhi, S.M.; Oilunkaniemi, R.; Laitinen, R.S.; Ahlgrén, M. The Reactions of Tellurium Tetrahalides with Triphenylphosphine under Ambient Conditions. *Inorg. Chem.* **2004**, *43*, 3742–3750. [CrossRef] [PubMed]
54. Chauhan, A.K.S.; Kumar, A.; Srivastava, R.C.; Butcher, R.J. Synthesis and characterization of monomeric diorganotellurium dihalides: Crystal and molecular structures of diphenacyltellurium dibromide and-diiodide. *J. Organomet. Chem.* **2002**, *658*, 169–175. [CrossRef]
55. Asahara, M.; Taomolo, S.; Tanaka, M.; Erabi, T.; Wada, M. Dependence of the rotational barrier of the Ar-group in RArTeX2 on the R-group [Ar = 2,6-(MeO)2C6H3; R = Me, Et, i-Pr; X = Cl, Br, I]. *Dalton Trans.* **2003**, 973–979. [CrossRef]
56. Hesford, M.J.; Levason, W.; Matthews, M.L.; Orchard, S.D.; Reid., G. Synthesis, characterisation and coordinating properties of the small ring S2Te-donor macrocycles [9]aneS2Te, [11]aneS2Te and [12]aneS2Te. *Dalton Trans.* **2003**, 2434–2442. [CrossRef]
57. Beckmann, J.; Dakternicks, O.; Duthic, A.; Mitchell, C.; Schurmann, M. Observation of Te···π and X···X Bonding in para-Substituted Diphenyltellurium Dihalides, (p-$Me_2NC_6H_4$)(p-YC_6H_4)TeX2 (X = Cl, Br, I., Y = H, EtO, Me_2N). *Aust. J. Chem* **2005**, *58*, 119–127. [CrossRef]
58. Chauhan, A.K.S.; Annmika; Kumar, A.; Srivnstava, R.C.; Butcher, R.J. Secondary bonding in functionalized organotellurium compounds: Preparation and structural characterization of bis(acetamido)tellurium(IV) diiodide and bis(4-methylbenzoylmethyl)tellurium(II). *J. Organomet. Chem.* **2005**, *690*, 313–321. [CrossRef]
59. Chauhan, A.K.S.; Anamika; Kumar, A.; Srivastava, R.C.; Butcher, R.J.; Beckmann, J.; Duthie, A. The interplay of secondary Te···N, Te···O, Te···I and I···I interactions, Te···π contacts and π-stacking in the supramolecular structures of [{2-(4-nitrobenzylideneamino)-5-methyl}phenyl](4-methoxyphenyl)tellurium dihalides. *J. Organomet. Chem.* **2005**, *690*, 1350–1355. [CrossRef]
60. Block, E.; Dikarev, E.V.; Glass, R.S.; Jin, J.; Li, B.; Li, X.; Zhang, S.-Z. Synthesis, Structure, and Chemistry of New, Mixed Group 14 and 16 Heterocycles: Nucleophile-Induced Ring Contraction of Mesocyclic Dications. *J. Am. Chem. Soc.* **2006**, *128*, 14949–14961. [CrossRef]
61. Srivastava, P.C.; Bajpai, S.; Bajpai, S.; Kumar, R.; Srivastava, S.; Butcher, R. Modification of supramolecular assemblies based on C4H7(CH3)Te heterocycle and cooperative participation of intermolecular I···I, Te···I, Te···O secondary bonds; C(sp^3)–H···O and C(sp^2)–H···O hydrogen bonds. *J. Struct. Chem.* **2007**, *18*, 223–230. [CrossRef]
62. Chauhan, A.K.S.; Singh, P.; Kumar, A.; Srivastava, R.C.; Butcher, R.J.; Duthic, A. Room-Temperature Insertion of Elemental Tellurium into the Csp3−Br and −I Bonds of α-Bromo- and α-Iodopinacolone. *Organometallics* **2007**, *26*, 1955–1959. [CrossRef]
63. Chauhan, A.K.S.; Singh, P.; Srivastavn, R.C.; Duthie, A.; Voda, A. Acylmethyl(aryl)tellurium(IV,II) derivatives: Intramolecular secondary bonding and steric rigidity. *Dalton Trans* **2008**, 4023–4028. [CrossRef] [PubMed]
64. Gurnani, C.; Levason, W.; Ratnani, R.; Reid, C.; Webster, M. Synthesis, characterisation and structures of thio-, seleno-and telluro-ether complexes of gallium (III). *Dalton Trans.* **2008**, 6274–6282. [CrossRef] [PubMed]
65. Groom, C.R.; Bruno, I.J.; Lightfoot, M.P.; Ward, S.C. The Cambridge Structural Database. *Acta Cryst.* **2016**, *B72*, 171–179. [CrossRef] [PubMed]
66. McCullough, J.D. Crystal and molecular structure of dibenzotellurophene diiodide $C_{12}H_8TeI_2$. *Inorg. Chem.* **1975**, *14*, 1142–1146. [CrossRef]
67. Srivastava, P.C.; Singh, V.; Dwivedi, S.; Butcher, R.J. Molecular and supramolecular structures of diethyltellurium diiodide and diethyltellurium bis(carboxylates). *Indian J. Chem.* **2010**, *A49*, 1197–1205.
68. Farran, J.; Alvarez-Larena, A.; Capparelli, M.V.; Piniella, J.F.; Germain, G. Torres-Castellanos, L. Two Polymorphs of Bis(4-methoxyphenyl)tellurium(IV) Diiodide. *Acta Cryst.* **1998**, *C54*, 995–1000.
69. Knight, F.R.; Fuller, A.L.; Buhl, M.; Slawin, A.M.Z.; Woollins, J.D. Hypervalent Adducts of Chalcogen-Containing peri-Substituted Naphthalenes; Reactions of Sulfur, Selenium, and Tellurium with Dihalogens. *Inorg. Chem.* **2010**, *49*, 7577–7596. [CrossRef]
70. Knight, F.R.; Arachchige, K.S.A.; Randall, R.A.M.; Buhl, M.; Slawin, A.M.Z.; Woollins, J.D. Exploring hypervalency and three-centre, four-electron bonding interactions: Reactions of acenaphthenechalcogen donors and dihalogen acceptors. *Dalton Trans.* **2012**, *41*, 3154–3165. [CrossRef]
71. Lang, E.S.; de Oliveira, G.M.; Silveira, E.T.; Burrow, R.A.; Vazquez-Lopez, E.M. Crystal and molecular structure of (α-naphthyl)TeI_3. *J. Organomet. Chem.* **2002**, *664*, 306–309. [CrossRef]
72. Desiraju, G.R.; Parthasarathy, R. The nature of halogen···halogen interactions: Are short halogen contacts due to specific attractive forces or due to close packing of nonspherical atoms? *J. Am. Chem. Soc.* **1989**, *111*, 8725–8726. [CrossRef]
73. Pedireddi, V.R.; Reddy, D.S.; Goud, B.S.; Craig, D.C.; Rae, A.D.; Desiraju, G.R. The nature of halogen ··· halogen interactions and the crystal structure of 1,3,5,7-tetraiodoadamantane. *J. Chem. Soc. Perkin Trans.* **1994**, *2*, 2353–2360. [CrossRef]
74. Fourmigué, M. Halogen bonding: Recent advances. *Curr. Opin. Solid State Mater. Sci.* **2009**, *13*, 36–45. [CrossRef]
75. Bauzá, A.; Frontera, A. Competition between lone pair-π, halogen-π and triel bonding interactions involving BX3 (X = F, Cl, Br and I) compounds: An ab initio study. *Theor. Chem. Acc.* **2017**, *136*, 37. [CrossRef]
76. Cavallo, G.; Metrangolo, P.; Milani, R.; Pilati, T.; Priimagi, A.; Resnati, G.; Terraneo, G. The Halogen Bond. *Chem. Rev.* **2016**, *116*, 2478–2601. [CrossRef] [PubMed]
77. Grabowski, S.J. Halogen bond with the multivalent halogen acting as the Lewis acid center. *Chem. Phys. Lett* **2014**, *605−606*, 131–136. [CrossRef]

78. Adhikari, U.; Scheiner, S. Sensitivity of pnicogen, chalcogen, halogen and H-bonds to angular distortions. *Chem. Phys. Lett.* **2012**, *532*, 31–35. [CrossRef]
79. Scheiner, S. Sensitivity of Noncovalent Bonds to Intermolecular Separation: Hydrogen, Halogen, Chalcogen, and Pnicogen Bonds. *CrystEngComm* **2013**, *15*, 3119–3124. [CrossRef]
80. Clark, T.; Hennemann, M.; Murray, J.S.; Politzer, P. Halogen bonding: The σ-hole. *J. Mol. Model.* **2007**, *13*, 291–296. [CrossRef]
81. Nziko, V.D.P.N.; Scheiner, S. Comparison of π-hole tetrel bonding with σ-hole halogen bonds in complexes of XCN (X = F, Cl,Br, I) and NH3. *Phys. Chem. Chem. Phys.* **2016**, *18*, 3581–3590. [CrossRef]
82. Scheiner, S. Characterization of Type I and II Interactions between Halogen Atoms. *Cryst. Growth Des.* **2022**, *22*, 2692–2702. [CrossRef]
83. Mukherjee, A.; Tothadi, S.; Desiraju, G.R. Halogen Bonds in Crystal Engineering: Like Hydrogen Bonds yet Different. *Acc. Chem. Res.* **2014**, *47*, 2514–2524. [CrossRef] [PubMed]
84. Nyburg, S.C.; Faerman, C.H. A revision of van der Waals atomic radii for molecular crystals: N, O, F, S, Cl, Se, Br and I bonded to carbon. *Acta Crystallogr. Sect. B Struct. Sci.* **1985**, *41*, 274–279. [CrossRef]
85. Nyburg, S.C. Intermolecular Forces and the Space Group of Solid Chlorine. *J. Chem. Phys.* **1964**, *40*, 2493–2501. [CrossRef]
86. Spilfogel, T.S.; Titi, H.M.; Friščić, T. Database Investigation of Halogen Bonding and Halogen···Halogen Interactions between Porphyrins: Emergence of Robust Supramolecular Motifs and Frameworks. *Cryst. Growth Des.* **2021**, *21*, 1810–1832. [CrossRef]
87. Bui, T.T.T.; Dahaoui, S.; Lecomte, C.; Desiraju, G.R.; Espinosa, E. The Nature of Halogen···Halogen Interactions: A Model Derived from Experimental Charge-Density Analysis. *Angew. Chem. Int. Ed.* **2009**, *48*, 3838–3841. [CrossRef]
88. Poropudas, M.J.; Vigo, L.; Oilunkaniemi, R.; Laitinen, R.S. Structural trends in TeI2RR′: Crystal structures and NMR spectra of $TeI_2(CH_2SiMe_3)_2$, $TeI_2Th(CH_2SiMe_3)$, $TeI_2Ph(CH_2SiMe_3)$, and TeI_2Th_2 (Th = 2-Thienyl, C_4H_3S). *Heteroat. Chem.* **2011**, *22*, 348–359. [CrossRef]
89. Knobler, C.; McCullough, J.D.; Hope, H. Crystal and molecular structure of 1-thia-4-telluracyclohexane 4,4-diiodide, $C_4H_8STeI_2$. *Inorg. Chem.* **1970**, *9*, 797–804. [CrossRef]
90. Torubaev, Y.V.; Samigullina, A.S. Long-Range Supramolecular Synthon Isomerism: Insight from a Case Study of Vinylic Tellurium Trihalides Cl(Ph)C=C(Ph)TeX3 (X = Cl, I). *Chemistry* **2022**, *4*, 196–205. [CrossRef]
91. Hope, H.; McCullough, J.D.; Knobler, C. Crystal and molecular structure of 1-oxa-4-telluracyclohexane 4,4-diiodide, C_4H_8OTeI2. *Inorg. Chem.* **1973**, *12*, 2665–2669. [CrossRef]
92. Shapovalov, S.S.; Pasynskii, A.A.; Skabitskii, I.V.; Tikhonova, O.G.; Kolos, A.V.; Grigor'ev, M.O. Chalcogenide Complexes of Cyclopentadienylnickel with Heterocyclic Carbene. *Russ. J. Coord. Chem.* **2018**, *44*, 647–652. [CrossRef]
93. Ahlrichs, R.; Bar, M.; Haser, M.; Horn, H.; Kolmel, C. Electronic structure calculations on workstation computers: The program system turbomole. *Chem. Phys. Lett.* **1989**, *162*, 165–169. [CrossRef]
94. Adamo, C.; Barone, V. Toward reliable density functional methods without adjustable parameters: The PBE0 model. *J. Chem. Phys.* **1999**, *110*, 6158–6169. [CrossRef]
95. Grimme, S.; Antony, J.; Ehrlich, S.; Krieg, H. A consistent and accurate ab initio parametrization of density functional dispersion correction (DFT-D) for the 94 elements H-Pu. *J. Chem. Phys.* **2010**, *132*, 154104. [CrossRef]
96. Weigend, F.; Ahlrichs, R. Balanced basis sets of split valence, triple zeta valence and quadruple zeta valence quality for H to Rn: Design and assessment of accuracy. *Phys. Chem. Chem. Phys.* **2005**, *7*, 3297–3305. [CrossRef] [PubMed]
97. Weigend, F. Accurate Coulomb-fitting basis sets for H to Rn. *Phys. Chem. Chem. Phys.* **2006**, *8*, 1057–1065. [CrossRef] [PubMed]
98. Bader, R.F.W. A quantum theory of molecular structure and its applications. *Chem. Rev.* **1991**, *91*, 893–928. [CrossRef]
99. Contreras-García, J.; Johnson, E.R.; Keinan, S.; Chaudret, R.; Piquemal, J.-P.; Beratan, D.N.; Yang, W. NCIPLOT: A program for plotting non-covalent interaction regions. *J. Chem. Theory Comput.* **2011**, *7*, 625–632. [CrossRef]
100. Humphrey, W.; Dalke, A.; Schulten, K. VMD: Visual molecular dynamics. *J. Mol. Graph.* **1996**, *14*, 33–38. [CrossRef]
101. Lu, T.; Chen, F. Multiwfn: A multifunctional wavefunction analyzer. *J. Comput. Chem.* **2012**, *33*, 580–592. [CrossRef]
102. Glendening, E.D.; Landis, C.R.; Weinhold, F. Natural bond orbital methods. *WIREs Comput. Mol. Sci.* **2012**, *2*, 1–42. [CrossRef]
103. Glendening, E.D.; Badenhoop, J.K.; Reed, A.E.; Carpenter, J.E.; Bohmann, J.A.; Morales, C.M.; Karafiloglou, P.; Landis, C.R.; Weinhold, F. *NBO 7.0: New Vistas in Localized and Delocalized Chemical Bonding Theory*; Theoretical Chemistry Institute, University of Wisconsin-Madison: Madison, WI, USA, 2018.
104. Kitaura, K.; Morokuma, K. A new energy decomposition scheme for molecular interactions within the Hartree-Fock approximation. *Int. J. Quantum Chem.* **1976**, *10*, 325–340. [CrossRef]
105. Batsanov, S.S. Van der Waals Radii of Elements. *Inorg. Mat.* **2001**, *37*, 871–885. [CrossRef]
106. Ivanov, D.M.; Bokach, N.A.; Kukushkin; Kukushkin, V.Y.; Frontera, A. Metal Centers as Nucleophiles: Oxymoron of Halogen Bond-Involving Crystal Engineering. *Chem. Eur. J.* **2022**, *18*, e202103173.
107. Soldatova, N.S.; Postnikov, P.S.; Ivanov, D.M.; Semyonov, O.V.; Kukurina, O.S.; Guselnikova, O.; Yamauchi, Y.; Wirth, T.; Zhdankin, V.V.; Yusubov, M.S.; et al. Zwitterionic iodonium species afford halogen bond-based porous organic frameworks. *Chem. Sci.* **2022**, *13*, 5650–5658. [CrossRef] [PubMed]
108. Kinzhalov, M.A.; Ivanov, D.M.; Melekhova, A.A.; Bokach, N.A.; Gomila, R.M.; Frontera, A.; Kukushkin, V.Y. Chameleonic metal-bound isocyanides: A π-donating CuI-center imparts nucleophilicity to the isocyanide carbon toward halogen bonding. *Inorg. Chem. Front.* **2022**, *9*, 1655–1665. [CrossRef]

109. Torubaev, Y.V.; Rozhkov, A.V.; Skabitsky, I.V.; Gomila, R.M.; Frontera, A.; Kukushkin, V.Y. Heterovalent chalcogen bonding: Supramolecular assembly driven by the occurrence of a tellurium(II)· · · Ch(I) (Ch = S, Se, Te) linkage. *Inorg. Chem. Front.* **2022**, *9*, 5635–5644. [CrossRef]
110. Artemjev, A.A.; Novikov, A.P.; Burkin, G.M.; Sapronov, A.A.; Kubasov, A.S.; Nenajdenko, V.G.; Khrustalev, V.N.; Borisov, A.V.; Kirichuk, A.A.; Kritchenkov, A.S.; et al. Towards Anion Recognition and Precipitation with Water-Soluble 1,2,4-Selenodiazolium Salts: Combined Structural and Theoretical Study. *Int. J. Mol. Sci.* **2022**, *23*, 6372. [CrossRef]
111. Sapronov, A.A.; Artemjev, A.A.; Burkin, G.M.; Khrustalev, V.N.; Kubasov, A.S.; Nenajdenko, V.G.; Gomila, R.M.; Frontera, A.; Kritchenkov, A.S.; Tskhovrebov, A.G. Robust Supramolecular Dimers Derived from Benzylic-Substituted 1,2,4-Selenodiazolium Salts Featuring Selenium· · · π Chalcogen Bonding. *Int. J. Mol. Sci.* **2022**, *23*, 14973. [CrossRef]
112. Sapronov, A.A.; Kubasov, A.S.; Khrustalev, V.N.; Artemjev, A.A.; Burkin, G.M.; Dukhnovsky, E.A.; Chizhov, A.O.; Kritchenkov, A.S.; Gomila, R.M.; Frontera, A.; et al. Se· · · π Chalcogen Bonding in 1,2,4-Selenodiazolium Tetraphenylborate Complexes. *Symmetry* **2023**, *15*, 212. [CrossRef]